PHYSICAL REVIEW B VOLUME 26, NUMBER 10 15 NOVEMBER 1982

Theory of static structural properties, crystal stability, and phase transformations: Application to Si and Ge

M. T. Yin* and Marvin L. Cohen
Department of Physics, University of California, Berkeley, California 94720
and Materials and Molecular Research Division, Lawrence Berkeley Laboratory,
Berkeley, California 94720

(Received 29 March 1982)

We demonstrate that not only the static structural properties but also the crystal stability and pressure-induced phase transformations in solids can be accurately described employing an *ab initio* pseudopotential method within the local-density-functional formalism. With the use of atomic numbers of constituent elements and a subset of crystal structures as the only input information, the calculated structural properties of Si and Ge are in excellent agreement with experiment.

I. INTRODUCTION

In this paper, we present an *ab initio* microscopic study of the static structural properties and other important structural properties including crystal stability and phase transformation of Si and Ge. Part of the results have been previously reported.[1] The method is based on a pseudopotential approach and uses the local-density-functional approximation[2] which has also been used in all-electron calculations of static structural studies of metals.[3]

We choose Si and Ge as our prototypes since they are the most studied semiconductors experimentally. Both have the (cubic) diamond structure and are found to undergo a semiconductor-metal phase transformation under pressure.[4] With the use of the x-ray diffraction technique, the transformed phases have been determined[5] to be of the tetragonal β-tin form. These structural transformations are accompanied by a large volume decrease[5] (22.7% for Si and 20.7% for Ge). Because of the difficulty in accurate pressure calibration, there has been some scattering of the data for the transition pressures.[6] The transition pressures were first measured[4] to be 150 kbar for Si and 105 kbar for Ge. The more recent values are 125 kbar for Si (Refs. 7 and 8) and 100 kbar for Ge.[9]

In addition to the diamond and β-tin phases, a hexagonal diamond phase has been made[10] for Si at room temperature and atmospheric pressure using a sequence of high-pressure and high-temperature treatments. This phase is semiconducting and has the same density as the (cubic) diamond phase. The axial ratio is 1.65, very close to the ideal value of 1.633. Since this form has not been found in nature and no large crystals have been prepared,[10] it is metastable with respect to the diamond phase. A similar structural form has not been found in Ge. There are other metastable phases of Si and Ge [a bcc form with 16 atoms per unit cell for Si (Ref. 10) and Ge (Ref. 11) and a tetragonal form with 12 atoms per unit cell for Ge (Ref. 12)]; these will not be considered in the present study.

There are interesting relations between the general phase transformation in semiconductors and other crystalline properties. Jamieson has related[5] the transition pressure (P_t) and the atomic volume change (ΔV) in the phase transformation to the fundamental energy gap (E_g), and he obtained an empirical rule of $P_t \Delta V = E_g/2$ for group-IV elements and isorow III-V compounds. Although this rule is less accurate when later refined experimental data is considered, the trend is still correct. This is consistent with the physical picture that the bigger the energy gap is, the more stabilized the structure is. Phillips[13] has suggested that ionicity may be an important parameter in characterizing the phase transformation. He noted that the rocksalt structure becomes more favorable as the high-pressure phase with increasing ionicity. The covalent counterpart of the rocksalt structure, that is, the simple cubic structure, is included in the present study.

Pressure-induced phase transformations in tetrahedrally coordinated semiconductors have previously been studied using information from electronic structure. Van Vechten observed[14] that the difference in total energy between the semiconducting diamond phase and the metallic β-tin phase is approximately equal to $\frac{1}{8}$ of the difference of the band-structure energies between the free-electron gas and the Penn model[15] evaluated at the experimental transition volume of the diamond phase. This, however, can only be regarded as an empirical relation. If accurate eigenvalues obtained from self-consistent band-structure calculations are used for the band-structure energies, the aforementioned relation no longer holds. A perturbative pseudopotential theory has been used[16] to calculate the thermodynamic parameters involved in the phase transformation. While good agreement with experiment was found in this approach, the error in energy incurred in the perturbative treatment especially when applied to the covalent phase may be of the order of the energy differences involved in the phase transformations (about a few tenths of an eV per atom). Besides, the theory introduced a potential parameter which is adjusted to fit the zero-pressure experimental volume. The sensitive dependence of the theory on that parameter is illustrated in a recent study[17] on the pressure-induced phase transformation of ZnSe with the use of a self-consistent pseudopotential theory. Without adjustment of the potential parameter, the rocksalt structure of ZnSe is calculated to be more stable than the zinc-blende structure in contradiction to the experimental observation. The theoretical results become consistent with experiment only after the parameter is adjusted to fit the experimental zero-pressure value.

In the following sections, we will first briefly discuss the *ab initio* pseudopotential approach[18] to the total-energy calculations (Sec. II). The procedures for pseudopotential construction and total-energy calculations are described in Sec. III. The results for Si and Ge, which will include (a) static structural properties, (b) crystal stability, (c) pressure-induced phase transformation, and (d) electronic structures, are presented and compared with experiment in Sec. IV. Final conclusions are given in Sec. V. We examine the accuracies of the calculated quantities with regard to various approximations used in the calculation in the appendices.

II. THEORY

In the present study, we use the *ab initio* pseudopotential approach[1] within the local-density-functional formalism.[2] This approach has been shown[19] to reproduce all-electron results faithfully. By focusing attention on the valence electrons which play a dominant role in the determination of structural properties, we are spared the computation of core states.

A plane-wave basis set is used to represent the (pseudo)valence wave functions. Such a basis set describes the charge density in the valence region to the same degree of accuracy for different crystal structures. In other words, the basis is not biased toward a particular crystal structure which is usually difficult to achieve in other choices of basis sets. Furthermore, the angular dependence of the charge density is well accounted for, and there is no need for a spherical averaging procedure of the charge density which may introduce appreciable error in describing highly directional covalent bonds.

The structural properties of solids are studied primarily through comparisons of total energies of systems under investigation. It is advantageous to perform the total-energy calculations in momentum space.[20] The total energy is given by

$$E_{\mathrm{tot}} = E_{\mathrm{kin}} + E'_{ec} + E'_{H} + E_{\mathrm{xc}}[\rho] + E'_{cc} \ . \tag{1}$$

The individual contributions can be interpreted as the electronic kinetic energy, the electron-core interaction energy, the electron-electron Coulomb energy, the electronic exchange and correlation energy, and the core-core Coulomb energy (the Ewald energy), respectively. Since the effect of core electrons are included in the pseudopotentials, the term "electrons" used in this paper refers to the valence electrons only. The prime in the second, third, and fifth terms on the right-hand side of Eq. (1) denotes that these terms are reduced finite quantities: Because of charge neutrality, the infinite contributions arising from the long-range Coulomb interaction cancel with one another and, thus, are excluded from these three terms.[20] $E_{\mathrm{xc}}[\rho]$ is a functional of charge density $\rho(\vec{r})$. In the local-density-functional approximation,

$$E_{\mathrm{xc}}[\rho] = \int \rho(\vec{r})\epsilon_{\mathrm{xc}}[\rho(\vec{r})]d\vec{r} \ , \tag{2}$$

where $\epsilon_{\mathrm{xc}}[\rho(\vec{r})]$ is a function of $\rho(\vec{r})$.

The individual terms (per cell) in Eq. (1) are given by

$$E_{\mathrm{kin}} = \frac{1}{N} \sum_{i,\vec{G}} n_i \,|\, \psi_i(\vec{k}_i + \vec{G}) \,|^2 \frac{\hbar^2 \,|\, \vec{k}_i + \vec{G} \,|^2}{2m} \ , \tag{3}$$

$$E'_{ec} = \frac{1}{N} \sum_{i,G,G'} n_i \psi_i^*(\vec{k}_i + \vec{G}) \psi_i(\vec{k}_i + \vec{G}') \left[V_{\mathrm{ps}}(\vec{k}_i + \vec{G}, \vec{k}_i + \vec{G}') + \delta_{\vec{G}\,\vec{G}'} \frac{1}{\Omega_c} \int_{\infty} \frac{Ze^2}{r} d\vec{r} \right] , \tag{4}$$

$$E'_H=\frac{\Omega_c}{2}\sum_{\vec{G}\neq 0}|\rho(\vec{G})|^2\frac{4\pi e^2}{|\vec{G}|^2}\ , \tag{5}$$

$$E_{\mathrm{xc}}=\frac{\Omega_c}{2}\sum_{\vec{G}}\rho^*(\vec{G})\epsilon_{\mathrm{xc}}(\vec{G})\ , \tag{6}$$

$$E'_{cc}=\tfrac{1}{2}\sum_{s,s'}Z_sZ_{s'}e^2\left\{\frac{4\pi}{\Omega_c}\sum_{\vec{G}\neq 0}\left[\frac{1}{|\vec{G}|^2}\cos[\vec{G}\cdot(\vec{\tau}_s-\vec{\tau}_{s'})]\exp\left[-\frac{|\vec{G}|^2}{4\eta^2}\right]\right]-\frac{\pi}{\eta^2\Omega_c}\right.$$
$$\left.+\sum_{\vec{l}}{}'\left[\frac{\mathrm{erfc}(\eta x)}{x}\right]_{x=|\vec{l}+\vec{\tau}_s-\vec{\tau}_{s'}|}-\frac{2\eta}{\sqrt{\pi}}\delta_{ss'}\right\}\ . \tag{7}$$

The symbols n_i, k_i, and ψ_i are, respectively, the occupation number, the crystal momentum, and the (pseudo)wave function in the momentum representation of state i. N is the total number of cells in the system, Ω_c is the cell volume, and $\vec{l}$ and $\vec{G}$ are the direct and reciprocal-lattice vectors. $Z\equiv\sum_s Z_s$, and Z_s and $\vec{\tau}_s$ are the core charge and the position vector for the sth atom in the basis. The symbol $\rho(\vec{G})$ is the Fourier transform of the (pseudo) valence charge density, and $V_{\mathrm{ps}}(\vec{k}_i+\vec{G},\vec{k}_i+\vec{G}')$ is the Fourier transform of the superposition of core pseudopotentials in momentum representation. The prime in the $\vec{l}$ summation in Eq. (7) excludes the $\vec{l}=0$ term when $\vec{\tau}_s=\vec{\tau}_{s'}$, and η is a parameter controlling the convergency of the Ewald summations.[21]

The momentum-space formalism is closely related to the plane-wave method for the calculation of electronic structures. The Schrödinger equation used in the plane-wave method can be easily derived variationally from the expression for the total energy in Eqs. (1)–(7). Using the resulting eigenvalues ϵ_i's, we obtain an alternative expression for the total energy

$$E_{\mathrm{tot}}=\frac{1}{N}\sum_i n_i\epsilon_i-E'_H+\Delta E_{\mathrm{xc}}+E'_{cc}\ , \tag{8}$$

where

$$\Delta E_{\mathrm{xc}}=\Omega_c\sum_{\vec{G}}\rho^*(\vec{G})[\epsilon_{\mathrm{xc}}(\vec{G})-V_{\mathrm{xc}}(\vec{G})] \tag{9}$$

and

$$V_{\mathrm{xc}}=\frac{d(\rho\epsilon_{\mathrm{xc}})}{d\rho}\ . \tag{10}$$

The double summation over $\vec{G}$'s in Eq. (4) is absorbed in the simple summation of the eigenvalues of the occupied states.

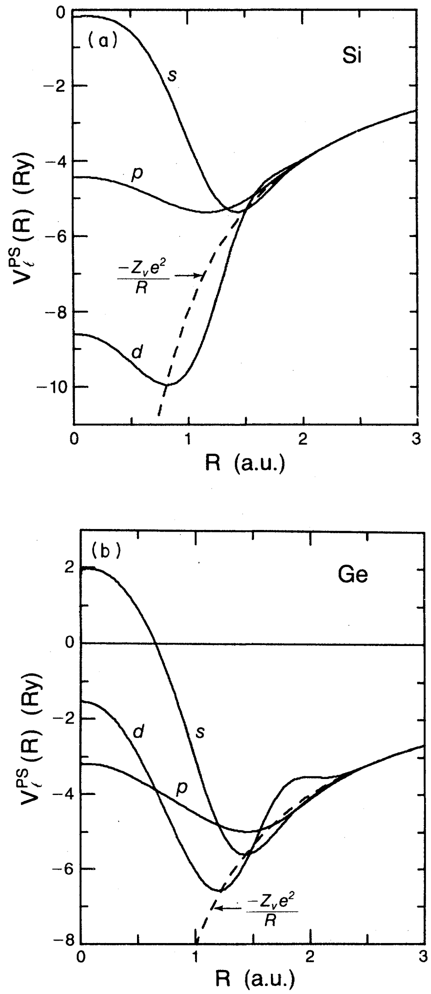

FIG. 1. *Ab initio* core pseudopotentials of (a) Si and (b) Ge generated using the reference valence configuration of $s^2p^{0.5}d^{0.5}$. The letters s, p, and d denote the nonlocal pseudopotential for angular momenta $l=0$, 1, and 2, respectively. Dashed line denotes the Coulomb potential of a (fictitious) pointlike atomic core.

III. CALCULATIONS

A. Pseudopotential construction

The *ab initio* pseudopotentials of Si (Ge) are generated through the Hamann-Schlüter-Chiang method[22] using the $3s^2 3p^{0.5} 3d^{0.5}$ ($4s^2 4p^{0.5} 4d^{0.5}$) reference configuration. The r_c values (in a.u.) chosen are 1.17, 1.35, and 1.17 (1.17, 1.36, and 1.36) for the *s*, *p*, and *d* components of the pseudopotential of Si (Ge). The reference configuration has a partially filled *d* orbital for the generation of the *d* pseudopotential. The nonlocal (angular-momentum-dependent) pseudopotentials of Si and Ge are shown in Fig. 1. The *d* pseudopotential of Ge is more repulsive than that of Si because Ge has 3*d* orbitals in the core and the 4*d* orbital of Ge is more extended than the 3*d* orbital of Si. The repulsive *d* pseudopotential of Ge pushes the *d* pseudo-orbital away from the core to simulate this effect. The Wigner interpolation formula[23] for the exchange and correlation energies is used for the present study.

The pseudopotentials thus generated are examined in the atomic limit. They are capable of reproducing the corresponding all-electron excitation energies and eigenvalues to within a few mRy and wave functions (outside the core region) to within 1% for atomic configurations over a wide energy range (about 2 Ry) above the atomic ground state. Examples are given in Table I and Fig. 2. Such agreement is a prerequisite for the solid-state calculations using the pseudopotential approximation[18] in which the interaction between the valence electrons and the atomic cores is approximated by pseudopotentials.

B. Total-energy calculations

For the present study, the total energy as a function of volume was calculated for seven crystal structures: the fcc, bcc, hcp, (cubic) diamond (CD), hexagonal diamond (HD), β-tin, and simple cubic (sc) phases. The first four phases encompass 80% of the observed elemental crystal structures. The HD phase is very similar to the CD phase. The β-tin phase is observed as a high-pressure form for Si and Ge. The simple cubic structure is a covalent counterpart of the NaCl structure. The ideal axial ratio ($c/a = \sqrt{8/3}$) is used for hcp and the HD structures. Several c/a ratios are used for the β-tin structure.

For each crystal structure of Si or Ge, we calculate the total energy at six to 15 different values of atomic volume ranging from 0.55 to 1.13 times the experimental value of the diamond phase (Ω_{expt}). For each value of atomic volume, the one-electron Schrödinger equation is solved iteratively to self-consistently[24] at which point the input and output screening potentials are identical to within 10^{-4} Ry, and E_{tot} is stable to within 10^{-5} Ry. The wave functions are expanded in a plane-wave basis set with a kinetic-energy cutoff (E_{pw}) of 11.5 Ry. Note that E_{pw} is kept constant for different atomic volumes and different crystal structures. In this way, the smallest wavelength of the plane waves used in the finite plane-wave expansion is approximately the same; namely, the spatial variations of wave functions are accounted for to similar accuracy. Furthermore, $\sqrt{E_{\text{pw}}}$ is a measure of the $\vec{k}$-space potential cutoff, that is, the extent to which the pseudopotential is sampled in $\vec{k}$ space. If E_{pw} is kept constant, the $\vec{k}$-space potential cutoff is practically the same for different atomic volumes and different crystal structures. This facilitates meaningful comparisons of total energies.

The number of sampling *k* points[25] used in the Brillouin-zone summation of the electronic density and total energy is increased until E_{tot} converges to the desirable accuracy as described below. For both the CD and HD phases the calculation yields semiconducting systems, and the absence of Fermi sur-

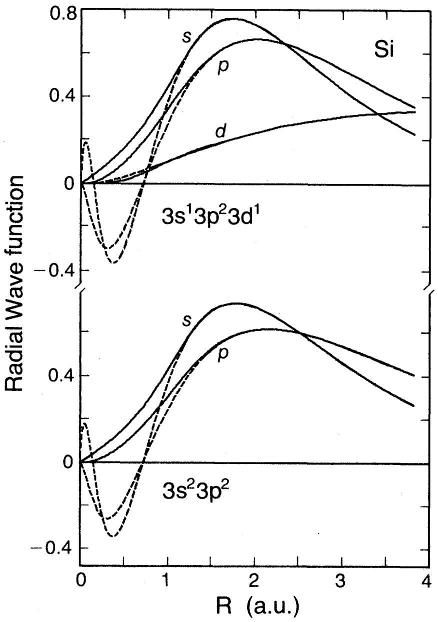

FIG. 2. Comparison between the pseudo (solid lines) and the corresponding all-electron (dashed lines) radial wave functions for the configurations $3s^2 3p^2$ and $3s^1 3p^2 3d^1$ of Si.

faces allows fast convergence for E_{tot} with respect to the number of sampling k points. Ten (six) special k points[25] in the irreducible Brillouin zone (IBZ) for the CD (HD) phase are sufficient to achieve 0.3 mRy/atom convergence for E_{tot}.

The other five phases are all found to be metallic in our calculation. A large number of k points are needed to account for the effects of the Fermi surface. The term most sensitive to the finite number of sampling k points in the total-energy calculation [Eq. (8)] is the Brillouin-zone summation of valence eigenvalues. A few sampling methods have been examined. They are as follows. (i) The linear tetrahedron method[26] in which the Brillouin zone is divided into tetrahedra. The eigenvalues are assumed to vary linearly within each tetrahedron, and this enables an analytic integration inside the tetrahedron. (ii) The discrete sampling method in which the Brillouin-zone summation is done in a straightforward manner using special k points.[25] (iii) The interpolation method in which the eigenvalues of a set of sampling k points are calculated directly from solving the Schrödinger equation, and the eigenvalues of a much larger set of k points are interpolated and used for the Brillouin-zone summation. The interpolation can be carried out through a Fourier-series expansion of the eigenvalues. We find that the convergence of the total energy with respect to the number of sampling k points is slow using the linear tetrahedral method. The errors come mainly from the linearization assumption. The convergence is faster if the discrete sampling method is used and even faster if the interpolation method is used.

As a numerical example, the convergent errors (in units of Ry/atom) caused by the finite number of sampling k points in the total-energy calculation of the fcc phase of Si at atomic volume $0.75\Omega_{\text{expt}}$ are 0.05 Ry/atom using 20 k points in the IBZ by the linear tetrahedron method and 0.005 and 0.001 Ry/atom using ten k points in the IBZ by the discrete sampling method and the interpolation method, respectively. The results presented in the following sections are obtained using the discrete sampling method.[27] For a convergence of 0.001 Ry/atom in total energy, the number of sampling k points in the IBZ are 24, 35, 70, 36, and 60 for the β-tin, sc, bcc, hcp, and fcc phases, respectively.

TABLE I. Eigenvalues and excitation energies of the pseudoatom for different atomic configurations of Si and Ge. Energies are in rydbergs. The method in Ref. 22 is employed to generate the pseudopotentials using $s^2p^{0.5}d^{0.5}$ reference configuration and Wigner correlation (Ref. 23). Values in parentheses are deviations from the corresponding all-electron results.

Configuration	Eigenvalues			Excitation energy
	s	p	d	(ΔE_{tot})
Si				
$3s^23p^2$	−0.7994	−0.3126		0
	(−0.0014)	(−0.0006)		
$3s^13p^3$	−0.8538	−0.3543		0.4932
	(−0.0008)	(−0.0004)		(0.0006)
$3s^13p^{2.5}3d^{0.5}$	−1.0226	−0.5048	−0.0380	0.7030
	(−0.0008)	(−0.0006)	(0.0001)	(0.0009)
$3s^23p^{0.5}3d^{0.5}$	−1.4851	−0.9420	−0.3364	(0.0009)
	(0.0000)	(0.0000)	(0.0000)	(0.0000)
$3s^23p^0$	−2.0948	−1.5154		1.7640
	(0.0028)	(0.0024)		(0.0005)
Ge				
$4s^24p^2$	0.8350	0.3061		0
	(−0.0015)	(−0.0008)		
$4s^14p^3$	0.9202	0.3533		0.5582
	(0.0001)	(−0.0006)		(0.0000)
$4s^14p^24d^1$	1.2155	0.6075	0.0607	1.0238
	(0.0017)	(0.0003)	(0.0000)	(0.0004)
$4s^24p^0$	2.1342	1.4745		1.7218
	(0.0030)	(0.0026)		(0.0002)

IV. RESULTS

A. Static structural properties

The static structural properties such as lattice constant, cohesive energy, and bulk modulus can be obtained from the calculated total energies as a function of volume for the observed crystal structure. We have calculated total energies of the cubic diamond structure of Si and Ge for 15 atomic volumes ranging from 0.55 to $1.13\Omega_{\text{expt}}$. They are then least-squares-fitted to Murnaghan's equation of state,[28(a)]

$$E_{\text{tot}}(V)=\frac{B_0 V}{B'_0}\left[\frac{(V_0/V)^{B'_0}}{B'_0-1}+1\right]+\text{const}\ , \tag{11}$$

where B_0 and B'_0 are the bulk modulus and its pressure derivative at the equilibrium volume V_0. This equation of state has been examined and found to be quite accurate for quite a few crystals under moderate compresssion.[28(b)] The minimum total energy (E_{min}), the equilibrium lattice constant, and the bulk modulus are readily deduced from the fitted parameters in the equation of state.[29] The cohesive energy is then the difference between the crystal energy which is the sum of E_{min} and the zero-point vibration energy and the total energy of the isolated pseudoatom with spin-polarization effects[30] included.

The calculated lattice constants, cohesive energies, and bulk moduli are compared with experiment[31–33] in Table II. The agreement is very good. These results also compare well with other *ab initio* calculations.[34] There have also been microscopic calculations of the static structural properties of Si (Ref. 35) and Ge [Ref. 35(a)] using pseudopotentials which are empirically fitted to the observed excitation spectra. These results are somewhat sensitive to the fitted pseudopotential, and the comparisons with experiment are not as good as the *ab initio* results. It is interesting to note that the band structures of *ab initio* calculations within the local-density-functional formalism cannot be used directly to compare with the excitation spectra; for example, the calculated indirect gap of Si is smaller than the experimental gap by a factor of 2 (see Sec. IV D).

TABLE II. Comparison of calculated and measured static properties of Si and Ge.

	Lattice constant (Å)	Cohesive energy (eV/atom)	Bulk modulus (Mbar)
Si			
Calculation	5.451	4.84	0.98
Experiment	5.429[a]	4.63[b]	0.99[c]
Ge			
Calculation	5.655	4.26	0.73
Experiment	5.652[a]	3.85[b]	0.77[c]

[a] Reference 31 (0 K).
[b] Reference 32 (0 K).
[c] Reference 33 (77 K).

The least-squares fit to the Murnaghan's equation of state has a rms error of about 10^{-4} Ry/atom. Other functional forms of the equation of state such as a polynomial form of the total energy as a function of the lattice constant, the volume, or their reciprocals have also been examined. The equilibrium lattice constant and E_{min} are rather insensitive to the functional form of the equation of state. The variations are 10^{-3} Å and 10^{-4} Ry/atom, respectively. In contrast, the bulk modulus (B_0) has a variation of about 10%, and its pressure derivative (B'_0) can vary by a factor of 2. The calculated values of B'_0 are 3.2 for Si and 3.7 for Ge using Murnaghan equation of state which compares well with the experimental values[33] of 4.2 for Si and 4.6 for Ge in view of the large theoretical uncertainty.

The above results are calculated using a plane-wave kinetic-energy cutoff E_{pw} of 11.5 Ry except for the cohesive energy to be discussed later. At this E_{pw}, the lattice constants converge to better than 1%, and the cohesive energies and the bulk moduli converge to about 5% (Appendix A). The dependence of the cohesive energy of Si on E_{pw} is shown in Fig. 3. As E_{pw} increases, the variational freedom of the wave functions becomes larger

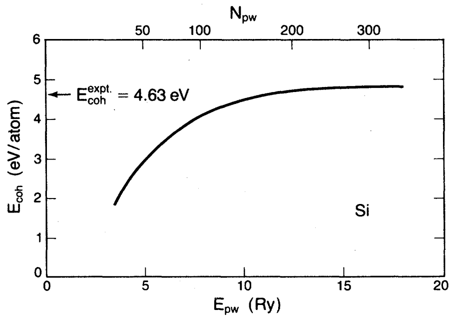

FIG. 3. Convergence test of the calculated cohesive energy (E_{coh}) of Si with respect to the kinetic-energy cutoff (E_{pw}) of the plane-wave basis set (N_{pw} is the approximate number of the plane waves in the basis set).

which gives rise to a lower total energy and a larger cohesive energy. The cohesive energy converges rapidly when E_{pw} is larger than 10 Ry. The calculated cohesive energies (per atom) for the case $E_{\text{pw}}=11.5$ Ry are 4.67 and 4.02 eV for Si and Ge, respectively, as compared to the almost fully converged values of 4.84 and 4.26 eV using $E_{\text{pw}}=20$ Ry (Table II). The differences in cohesive energy between theory and experiment are 0.21 eV for Si and 0.41 eV for Ge. The pseudopotential approximation[18] accounts for errors of the order of 0.05 eV.[19] The remaining portion of the errors seems to come from the local-density-functional approximation[2] and the functional form of the exchange-correlation energy, especially for the atomic calculations.[36] Even with the spin-polarization effect included in the fashion described in Ref. 30 in the atomic calculations, the calculated ionization potentials of atoms differ from the experimental values by a few tenths of an eV.[30]

Comparison of various energy contributions to the total energy between an isolated atom and a crystalline atom for Si and Ge are given in Table III. The term E_{pot} is the sum of E'_{ec}, E'_{H}, and E'_{cc} [Eq. (15)]. The term E_{spin} is the energy gain resulting from spin polarization of the atom. It is calculated by taking the total-energy difference between the spin-polarized and the unpolarized pseudoatoms with the valence configuration s^2p^2 where the form of the exchange-correlation energy proposed by Gunnarsson and Lundqvist[30] is used. The term E_{vib} is the zero-point vibrational energy estimated from measured phonon frequencies.[37] As the crystals form, the electrons become localized to form chemical bonds, which gives rise to an increase in electronic kinetic energy (E_{kin}) and decreases in potential energies (E_{xc} and E_{pot}). We note that both E_{xc} and E_{pot} are essential in stabilizing the crystal. In the absence of either one, the crystal would become unstable. The contributions from E_{spin} and E_{vib} tend to favor the isolated atom, but their effects are not dominant.

Shown in Fig. 4 are contour plots of pseudovalence charge densities of Si and Ge in the (110) plane. Because of the norm-conserving property of *ab initio* pseudopotentials, the pseudovalence charge distributions are expected to faithfully reproduce real valence charge distributions outside the core region, and there is no need for core orthogonalization. The contour plots for Si and Ge look rather similar.[38] The contour lines in the bonding region are elongated along the bonding direction, which agrees with the experimental valence charge density of Si synthesized[39] from the x-ray data.[40]

TABLE III. Comparison of various energy contributions (in units of Ry/atom) to the total energy between the (pseudo)atom and the crystal for Si and Ge.

	Atom	Crystal	Diff.
Si			
E_{kin}	2.518	3.015	0.497
E_{xc}	-1.926	-2.381	-0.455
E_{pot}	-9.095	-8.555	-0.460
E_{spin}	-0.058	0	0.058
E_{vib}	0	0.005	0.005
E_{tot}	-7.561	-7.916	-0.355
Ge			
E_{kin}	2.511	2.844	0.333
E_{xc}	-1.910	-2.312	-0.402
E_{pot}	-8.135	-8.438	-0.303
E_{spin}	-0.056	0	0.056
E_{vib}	0	0.003	0.003
E_{tot}	-7.590	-7.903	-0.313

We have calculated the x-ray structural factors of Si and Ge by adding the core structural factors to the valence structural factors obtained in crystalline calculations. The core structural factors are obtained from atomic calculations with the valence configuration of s^2p^2. They differ from the corresponding results using valence configuration sp^3 by at most 0.006 e/cell, which demonstrates the inertness of the core electrons as the valence configuration changes. A comparison between calculated x-ray structural factors with experiment[40–42] for Si and Ge are given in Table IV. (The experimental values in Table IV have been corrected for the Debye-Waller factor and anomolous dispersion effects.) The agreement is very good. We note that

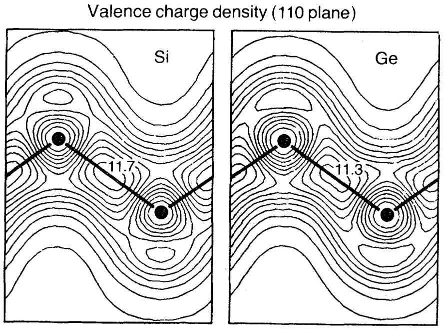

FIG. 4. Contour plots of the valence charge density in the (110) plane of the cubic diamond (CD) phase of Si and Ge at Ω_{expt} (Ref. 31). Charge density is in units of electrons per atomic volume with a contour step of 1. The black dots denote the atomic positions and straight lines denote the atomic chains.

TABLE IV. Comparison of calculated x-ray structure factors for Si and Ge with experiment (in units of electron per primitive cell).

	Si		Ge	
	Theory	Expt.[a]	Theory	Expt.[b]
000	28.00	(28.00)	64.00	(64.00)
111	15.13	15.19	38.85	39.42
220	17.23	17.30	47.26	47.44
311	11.28	11.35	31.24	31.37
222	0.34	0.38	0.28	0.27
400	14.76	14.89	40.47	40.50
331	10.11	10.25	27.37	27.72
422	13.22	13.42	35.84	36.10
333	8.92	9.09	24.26	24.50
511	8.96	9.11	24.28	
440	11.88	12.08	32.14	32.34

[a] References 40 and 41.
[b] Reference 42.

the (222) reflection, which is forbidden in a simple superposition of atomic charge densities, is well accounted for. Our results agree well with other *ab initio* calculations.[34(b),43–45] The smaller values of the (222) reflection calculated in Ref. 45 may be due to the limited number of Gaussian-type orbitals used in the wave-function expansion.

B. Crystal stability

As described in Sec. III B, total energies at several different lattice constants are calculated for seven crystal structures: the fcc, bcc, hcp, sc, CD, HD, and β-tin phases. These data are then least-squares-fitted to the Murnaghan equation of state.[27] The fitted total-energy curves as a function of atomic volume for the seven phases of Si and Ge are shown in Figs. 5 and 6. The minimum total energy per atom ($E_{\min}$), the relative total energy difference $\Delta E_{\min}$ ($\equiv E_{\min} - E_{\min}^{\mathrm{CD}}$), and the corresponding atomic volume ($V_{\min}$) for each phase of Si and Ge are given in Table V. We note that the value of E_{pw} controlling the plane-wave expansion is 11.5 Ry. For this value, the difference $\Delta E_{\min}$ between phases has already converged to 0.001

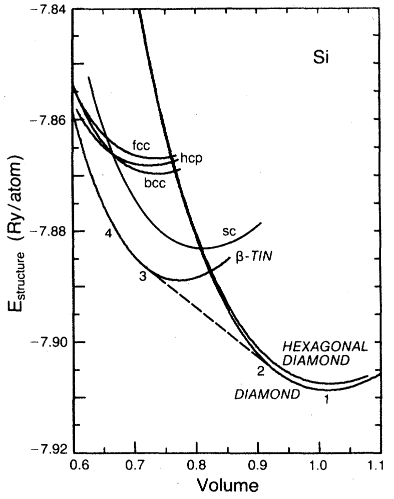

FIG. 5. Total-energy curves of the seven phases of Si as a function of the atomic volume normalized to Ω_{expt} (Ref. 31). Dashed line is the common tangent of the energy curves for the diamond phase and the β-tin phase ($c/a = 0.552$).

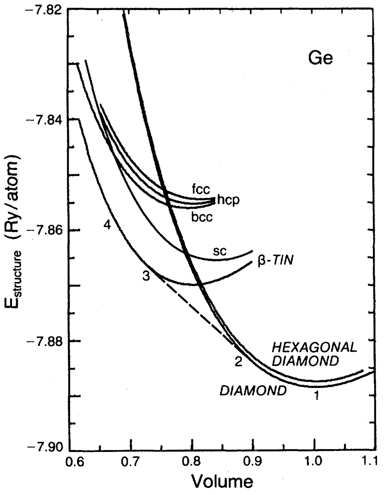

FIG. 6. Total-energy curves of the seven phases of Ge as a function of the atomic volume normalized to Ω_{expt} (Ref. 31). Dashed line is the common tangent of the energy curves for the diamond phase and the β-tin phase ($c/a = 0.551$).

TABLE V. Volumes at the minimum structural energies ($V_{\min}$, normalized to measured free volume), the minimum energies ($E_{\min}$), and $\Delta E_{\min}$ $(\equiv E_{\min} - E_{\min}^{\text{diamond}})$ for the seven plausible structures of Si and Ge.

	Diamond	Hexagonal diamond	β-tin	sc	bcc	hcp	fcc
Si							
$V_{\min}$	1.012	1.015	0.773	0.808	0.736	0.723	0.733
$E_{\min}$ (Ry)	-7.9086	-7.9074	-7.889	-7.883	-7.870	-7.868	-7.867
$\Delta E_{\min}$ (eV)	0	0.016	0.27	0.35	0.53	0.55	0.57
Ge							
$V_{\min}$	1.003	1.003	0.802	0.839	0.795	0.805	0.816
$E_{\min}$ (Ry)	-7.8885	-7.8874	-7.870	-7.866	-7.856	-7.855	-7.854
$\Delta E_{\min}$ (eV)	0	0.015	0.25	0.31	0.44	0.45	0.46

eV/atom while the absolute magnitude of $E_{\min}$ converges to only 0.02 eV/atom (Sec. VI A). Here we neglect the contribution from the zero-point vibration which has only small effects on the results to be reported.

The values for the β-tin phase given in Table VI and Figs. 5 and 6 are calculated using the experimental axial ratio[5] (0.5516 for Si and 0.5512 for Ge). Total-energy calculations have also been done for β-tin phases of different axial ratios (to be discussed in detail in the next subsection). From these calculations of the total energies of the seven phases, we find that the CD phase has the lowest $E_{\min}$ and is, thus, the most stable phase among the seven phases of Si and Ge. This is in agreement with experimental observation.

Compared to the CD phase, the HD phase has similar tetrahedral bonding character and differs only in the positions of the third nearest neighbors. It is expected that total energies for the two phases should be very close. Our calculations are not only consistent with this observation but they also show that the CD phase is more stable by a small energy difference (0.016 and 0.015 eV/atom for Si and Ge). The contour plot of valence charge density of the HD phase of Si at Ω_{expt} is shown in Fig. 7. The charge distribution is quite similar to that of the CD phase (Fig. 4).

For both Si and Ge, the other five phases are metallic and have $E_{\min}$ a few tenths of an eV per atom higher than the CD phase. The ordering of phases as $E_{\min}$ increases is β-tin, sc, bcc, hcp, and fcc. The $V_{\min}$'s (normalized to Ω_{expt}) of the metallic phases of Ge are larger than those of Si. This results from the filled $3d$ bands in Ge which exert a Pauli-type repulsion on the valence electrons having d-like character as manifested by the more repulsive d pseudopotential of Ge (Fig. 1). This effect is more appreciable in the metallic phases than in the sp^3-bonded CD and HD phases.

Values of $\Delta E_{\min}$ of a few metallic phases of Si and Ge have been estimated from thermodynamical data. They are (in units of eV/atom) 0.46 and 0.53 for the bcc and hcp phases of Si [Ref. 46(a)] and 0.29 and 0.37 for the β-tin and fcc phases of Ge,[46(b)] respectively. These empirical values compare very well with our results (Table V). We note that the crystal stability of Si has been reported in Ref. 35(c)

TABLE VI. Comparison between various contributions to the total energy of the cubic diamond (CD) and the hexagonal diamond (HD) phase at Ω_{expt} (Ref. 31). Energies are in units of Ry/atom. E_e is the electronic contribution which is the sum of E_{kin}, E_{xc}, E'_H, and E'_{ec}.

		Si			Ge	
	CD	HD	CD-HD	CD	HD	CD-HD
E_{kin}	3.0001	3.0007	-0.0006	2.8295	2.8311	-0.0016
E_{xc}	-2.3782	-2.3784	0.0002	-2.3096	-2.3100	0.0004
E'_H	0.5322	0.5435	-0.0113	0.5471	0.5587	-0.0116
E'_{ec}	-0.6632	-0.6861	0.0229	-0.8920	-0.9156	0.0236
E_e	0.4909	0.4797	-0.0112	0.1750	0.1642	-0.0108
E'_{cc}	-8.3995	-8.3871	-0.0124	-8.0634	-8.0516	-0.0118
E_{tot}	-7.9086	-7.9074	-0.0012	-7.8884	-7.8874	-0.0010

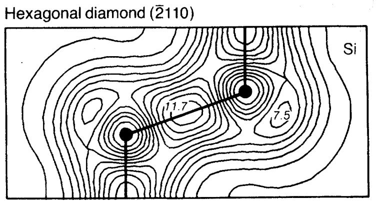
Hexagonal diamond ($\bar{2}110$)

FIG. 7. Contour plot of the (valence) charge density in the ($\bar{2}110$) plane of the hexagonal diamond phase of Si at Ω_{expt} (conventions of Fig. 4).

using a pseudopotential empirically fitted to excitation spectra. The diamond phase was found to be more stable than the β-tin, bcc, hcp, and fcc phases. However, the ΔE_{min}'s between phases reported in Ref. 35(c) differ from the present results and the thermodynamically derived results.[46(a)]

Since the structural properties of Si and Ge are qualitatively similar, we will concentrate on the results of Si in the following discussion. The contour plots of valence charge densities of the CD phase and the five metallic phases of Si at $0.751\Omega_{\text{expt}}$ are shown in Fig. 8. (The contour plot for the HD phase is not shown because it is quite similar to that of the CD phase.) The maximum valence charge density between nearest neighbors is a useful scale to gauge the covalent character: The CD and HD phases have large values of maximum valence charge density and, thus, strongly covalent character. Next come the β-tin and sc phases. The bcc, fcc, and hcp phases have the least covalent character. Notice the existence of prominent bond charge in the CD (as well as HD), β-tin, and sc phases.

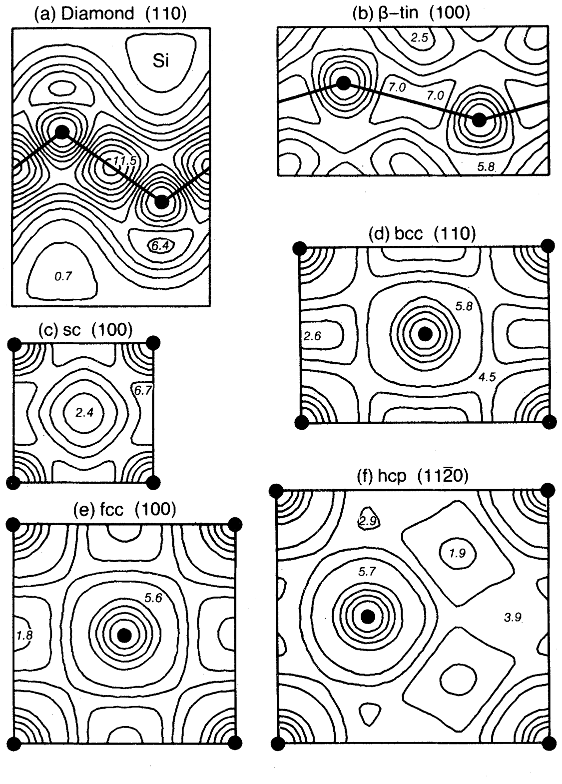
(a) Diamond (110)
(b) β–tin (100)
(c) sc (100)
(d) bcc (110)
(e) fcc (100)
(f) hcp ($11\bar{2}0$)

FIG. 8. Charge density contour plots of six phases of Si at $0.751\Omega_{\text{expt}}$ (conventions of Fig. 4).

The valence charge distribution around the atoms in the close-packed phases are reminiscent of the valence charge distribution in the atom. In fact, the charge density resulting from a superposition of atomic valence charge densities has similar peak positions and values. Figure 9 shows contour plots of the charge density so obtained[47] in the (110) plane for the bcc phase of Si at $0.751\Omega_{\text{expt}}$ and its difference from the corresponding self-consistent result (see Fig. 8). As the crystal forms, there is small charge pileup between nearest neighbors. This effect becomes bigger as the covalent character increases. We note in passing that the charge distribution in the close-packed phases is quite spherically symmetric around the atoms, and this supports the use of spherical averaging procedures for close-packed crystals in some band-structure methods such as the augmented-plane-wave method.[48]

It is instructive to compare the contributions to the total energy [Eq. (1)] for different phases. The comparison of the individual energy contributions between the CD and the HD phases of Si and Ge at Ω_{expt} are shown in Table VI. The energy terms E_{kin}, E'_H, and E'_{cc} favor the CD phase while E_{xc} and E'_{ec} favor the HD phase. The signs of E'_H, E'_{cc}, and

(a) bcc (110) LCAC

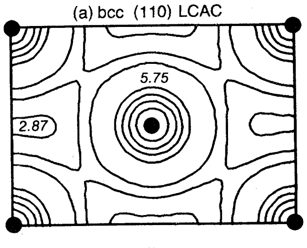

(b) Difference

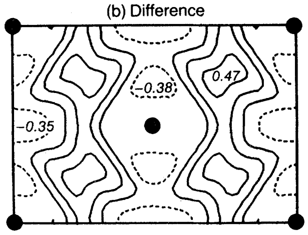

FIG. 9. (a) Contour plot of the charge density of the bcc phase of Si at $0.751\Omega_{\text{expt}}$ constructed from a superposition of pseudoatomic charge densities. (b) Contour plot of the difference between Figs. 8(d) and 9(a) (conventions of Fig. 4).

TABLE VII. Comparison of various contributions to the total energy [Eq. (1)] for the diamond, sc, β-tin, bcc, hcp, and fcc phases of Si (at $0.751\Omega^{\rm Si}_{\rm expt}$) and Ge (at $0.742\Omega^{\rm Ge}_{\rm expt}$). Energies are in units of Ry/atom. E_e is the electronic contribution, which is the sum of $E_{\rm kin}$, $E_{\rm xc}$, E'_H, and E'_{ec}.

	Diamond	sc	β-tin	bcc	hcp	fcc
Si $(0.751\Omega_{\rm expt})$						
$E_{\rm kin}$	3.4195	3.1081	3.0674	2.9896	2.9855	2.9855
$E_{\rm xc}$	−2.5366	−2.4379	−2.4283	−2.4037	−2.4033	−2.4035
E'_H	0.4200	0.1121	0.0842	0.0332	0.0351	0.0356
E'_{ec}	0.0736	1.0698	1.1928	1.4199	1.4229	1.4235
E_e	1.3764	1.8520	1.9162	2.0390	2.0397	2.0412
E'_{cc}	−9.2394	−9.7330	−9.8046	−9.9085	−9.9075	−9.9079
$E_{\rm tot}$	−7.8630	−7.8809	−7.8884	−7.8695	−7.8678	−7.8667
Ge $(0.742\Omega_{\rm expt})$						
$E_{\rm kin}$	3.2103	2.9414	2.9035	2.8468	2.8470	2.8456
$E_{\rm xc}$	−2.4651	−2.3713	−2.3507	−2.3378	−2.3380	−2.3377
E'_H	0.4237	0.1266	0.0955	0.0451	0.0477	0.0477
E'_{ec}	−0.1138	0.8225	0.9421	1.1395	1.1373	1.1401
E_e	1.0551	1.5191	1.5803	1.6935	1.6940	1.6957
E'_{cc}	−8.9034	−9.3791	−9.4481	−9.5482	−9.5472	−9.5476
$E_{\rm tot}$	−7.8483	−7.8600	−7.8678	−7.8546	−7.8532	−7.8518

E'_{ec} can be explained qualitatively by the observation that the distance to the third nearest neighbor is longer in the CD phase than in the HD phase. The values of E'_H and E'_{cc} are close, and they are almost canceled by E'_{ec}. A slightly more localized charge distribution in the HD phase (see Figs. 4 and 7) seems to be the reason for the larger absolute magnitudes of $E_{\rm kin}$ and $E_{\rm xc}$ for the HD phase. (The computational error in the differences of the various energy contributions and the total energies is about 0.0003 Ry/atom.) Since the total energy differences are of the same order as or even smaller than the various energy terms, all energy terms are important in determining which of the CD and HD phases is more stable.

Incidentally, the structural relation between the cubic ZnS and hexagonal ZnS phases of ionic semiconductors is the same as that between the CD and HD phases of covalent semiconductors. The difference in Ewald energy (E'_{cc}) between the hexagonal form and the cubic form is reduced (in favor of the hexagonal form) by 0.0007 Ry/atom for the III-V compounds and 0.003 Ry/atom for the II-VI compounds with respect to the covalent counterpart at the measured Si volume. These values are comparable to the total-energy difference between the CD and HD phases of Si and Ge. The favorable gain in the Ewald energy seems to be the reason why stable hexagonal ZnS structures are found in the II-IV compounds, for example, CdS, ZnS, and ZnSe.

The individual contributions to the total energy for the diamond, sc, β-tin, bcc, hcp, and fcc phases of Si (at $0.751\Omega^{\rm Si}_{\rm expt}$) and Ge (at $0.742\Omega^{\rm Ge}_{\rm expt}$) are given in Table VII. Note that the change of the energy contributions between different phases correlates quite well with the nearest-neighbor distance, which in turn is closely related to the coordination number. The coordination numbers are 4, 6, 6, 8, 12, and 12, and the relative nearest-neighbor distances at the same atomic volume are 1, 1.155, 1.159, 1.260, 1.296, and 1.296 for the diamond, sc, β-tin, bcc, hcp, and fcc phases, respectively. (The β-tin phase has four nearest neighbors and two second-nearest neighbors at a 6% larger distance.) As the coordination number becomes smaller, the nearest-neighbor distance will usually become smaller if the atomic volume is kept the same. This causes a larger charge pileup between nearest neighbors and a more localized valence charge distribution (Fig. 7). Thus, $E_{\rm kin}$ and E'_H will increase, $E_{\rm xc}$ and E'_{ec} will decrease, and the sum of these four terms [called the electronic contribution (E_e)] will decrease. The Ewald contribution (E'_{cc}), however, will usually increase because of the larger electrostatic potential energy between neighboring atomic cores. In other words, the electronic contribution favors phases of low coordination numbers while the Ewald contribution favors phases of high coordination numbers. Here the bcc, hcp, and fcc phases are regarded as one entity because their energy contributions are very close.

The total energies of the phases depend on the detailed balance between the electronic and the Ewald contributions. At the particular atomic volumes of

TABLE VIII. Comparison of the calculated and measured transition volumes ($V_t^{d,\beta}$) of the diamond and β phases, their ratios (V_t^β/V_t^d), and the transition pressures (P_t) for Si and Ge. Volumes are normalized to the measured zero-pressure volumes (Ref. 31).

	V_t^d	V_t^β	V_t^β/V_t^d	P_t (kbar)
Si				
Calculation	0.928	0.718	0.774	99
Experiment	0.918[a]	0.710[a]	0.773[a]	125[b]
Deviation	1.1%	1.1%	0.1%	−20%
Ge				
Calculation	0.895	0.728	0.813	96
Experiment	0.875[a]	0.694[a]	0.793[a]	100[c]
Deviation	2.3%	4.9%	2.5%	−4%

[a] Reference 5.

[b] References 7 and 8.

[c] Reference 9.

Si and Ge (Table VIII), the relatively high Ewald contribution causes the total energy of the diamond phase to be higher than those of other phases. Consequently, a phase transformation will occur before the diamond phase of Si or Ge, which is the most stable phase at zero pressure, is compressed to such small volumes. This topic will be discussed in the next subsection.

C. Pressure-induced phase transformation

It is a well-known thermodynamic theorem that the phase transformation occurs when the Gibbs free energy,

$$G \equiv E_{\text{tot}} + PV - TS , \tag{12}$$

becomes equal between the two phases. By applying this theorem to the zero-temperature case considered here, it is easily shown that the pressure-induced phase transformation occurs along the common tangent line between the $E_{\text{tot}}(V)$ curves of the two phases under consideration and the negative of the slope of the common tangent line is the transition pressure (P_t).

Although the HD phase of Si or Ge has the second lowest $E_{\min}$, the common tangent between the HD and the CD energy curves either does not exist or has a slope much larger than that between the β-tin and the CD energy curves. Consequently, the HD phase is not the phase the CD phase will transform to under pressure. Since the HD energy curve lies slightly higher than the CD energy curve, the HD phase is a metastable phase having an equilibrium volume very close to that of the CD phase (Table V). The HD phase of Si has been experimentally observed[10] to be metastable. Our calculated equilibrium volume for the HD phase is in excellent agreement with experiment.[10]

As can be seen from Figs. 5 and 6, the phase transformation to the β-tin phase has the smallest transition pressure among the possible pressure-induced phase transformations from the CD phase of Si or Ge. Thus our calculations show that under increasing hydrostatic pressure, the CD phase of Si or Ge will transform to the β-tin phase among the six possible choices for the transformed phase.

With increasing applied hydrostatic pressure, the crystals of Si and Ge will follow the path $1 \rightarrow 2 \rightarrow 3 \rightarrow 4$ as shown in Figs. 5 and 6. The phase transformation occurs along the path $2 \rightarrow 3$. This segment represents a mixture of these two phases. The initial and final transition volumes (V_t^d and V_t^β) are determined from the tangent points. The calculated transition volumes and transition pressures of Si and Ge are given in Table IX along with the experimental values.[5,7–9] The agreement for the transition volumes are excellent. The differences between theory and experiment are only a few percent.

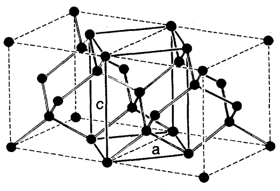

FIG. 10. Ball-and-stick model for the diamond crystal structure. Dashed lines denote the cubic unit cells and solid lines denote the tetragonal unit cell.

TABLE IX. Eigenvalues of Si and Ge in eV at Γ, X, and L calculated using $E_{\rm pw}=11.5$ and 20 Ry, which correspond to about 180 and 400 plane waves, respectively. Energies in eV are measured from the valence-band maximum ($\Gamma_{25'}$).

	Si		Ge	
$E_{\rm pw}$	11.5 Ry	20 Ry	11.5 Ry	20 Ry
Γ_1	11.95	−11.93	−12.48	−12.48
$\Gamma_{25'}$	0	0	0	0
Γ_{15}^c	2.54	2.53	2.53	2.55
$\Gamma_{2'}^c$	3.39	3.29	1.01	0.73
Γ_1^c	7.66	7.63	6.45	6.41
X_1	−7.80	−7.78	−8.58	−8.57
X_4	−2.92	−2.88	−3.08	−3.04
X_1^c	0.62	0.61	0.71	0.73
X_3^c	9.99	9.97	9.53	9.54
$L_{2'}$	−9.57	−9.52	−10.39	−10.36
L_1	−7.01	−7.00	−7.42	−7.41
$L_{3'}$	−1.23	−1.20	−1.41	−1.39
L_1^c	1.52	1.48	0.51	0.47
L_3^c	3.37	3.31	3.67	3.70
$L_{2'}^c$	7.48	7.48	6.96	6.99

The transition pressures have a larger discrepancy. While the calculated transition pressures are for zero temperature, the experimental transition pressures were measured at room temperature.[7–9] Using the phase diagrams shown in Ref. 49, we estimate that the transition pressure may change by $\lesssim \pm 15\%$ from room temperature to 0 K. In addition, possible superstress effects may cause the measured value to be higher than the theoretical value and the theoretical value itself has a large uncertainty (Appendix C). Thus, the agreement of the calculated transition pressures with experiment is considered to be quite satisfactory.

There is an interesting structural relationship between the CD phase and the β-tin phase. Shown in Fig. 10 is a ball-and-stick model of the diamond crystal structure in dashed cubic cells. A tetragonal unit cell can equally well be chosen to represent the crystal structure as indicated by solid lines in Fig. 10. The space lattice of the diamond crystal structure is then body-centered tetragonal with an axial ratio (c/a) of $\sqrt{2}$. The observed β-tin phases belong to the same lattice class but with a much smaller axial ratio [0.552 for Si (Ref. 5), 0.551 for Ge (Ref. 5), and 0.546 for the real β-tin (Ref. 31)].

Calculations have been carried out for several β-tin structures of Si and Ge with axial ratios varied within 20% of the observed values. The calculated total-energy curves of Si for the diamond phase and the β-tin phases with axial ratios 0.458, 0.488, 0.552, and 0.621 are shown in Fig. 11. The energy curve with axial ratio 0.46 lies above the other curves. As the axial ratio increases, the energy curve moves downward. After the axial ratio reaches the value 0.55, the energy curve moves upward again. It is clear from Fig. 11 that the transformed β-tin phase under hydrostatic pressure has axial ratio close to 0.55. When we vary the axial ratio within 5% of the value 0.55, the calculated total-energy curves differ from each other by less

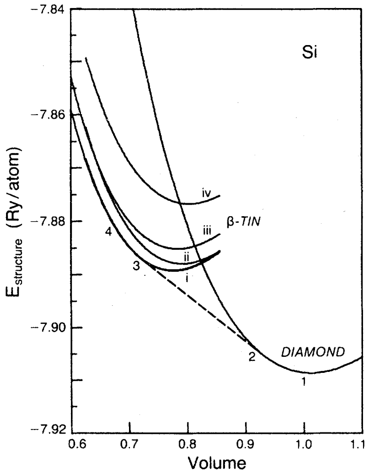

FIG. 11. Total-energy curves of the diamond phase and the β-tin phases with axial ratios (i) 0.552, (ii) 0.621, (iii) 0.488, and (iv) 0.458 as a function of the atomic volume normalized to $\Omega_{\rm expt}$. Dashed line is the common tangent of the energy curves for the diamond phase and the β-tin phase (i).

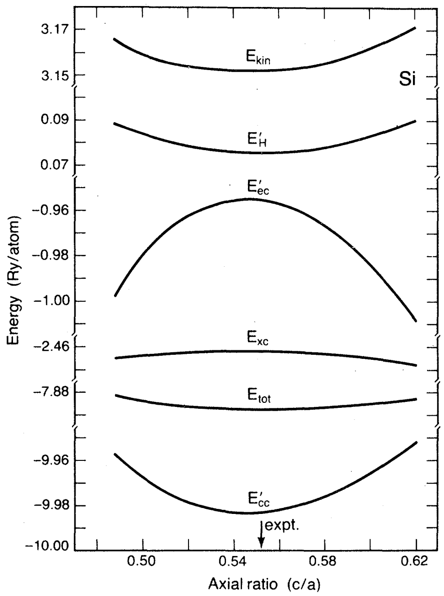

FIG. 12. Individual energy contributions of the β-tin phase of Si as a function of the axial ratio at a fixed atomic volume of $0.71\Omega_{\text{expt}}$. (The contribution E'_{ec} has a constant 2.285 subtracted out.)

than 0.4 mRy/atom and are essentially indistinguishable from the curve (i) if drawn in Fig. 11. Consequently, the theoretical estimate of the axial ratio of the pressure-transformed β-tin phase of Si is $0.55\pm5\%$. A similar treatment has also been done for Ge. The calculated axial ratio is also $0.55\pm5\%$. These values agree quite well with the experimental values[5] of 0.552 (Si) and 0.551 (Ge).

It is instructive to analyze the individual energy contributions to the total energy as the axial ratio of the β-tin phase varies. Figure 12 shows the individual energy contributions and total energy of the β-tin phase of Si as a function of the axial ratio at a fixed atomic volume $(0.71\Omega_{\text{expt}})$. The minimum of the Ewald energy (E'_{cc}) has an axial ratio of 0.5445 at which the second-nearest-neighbor distance is very close to the nearest-neighbor distance and the effective coordination number is 6 instead of 2 or 4. It is a rule of thumb that the Ewald energy favors high coordination numbers and evenly distributed atoms in the crystal. The total energy also has a minimum close to the axial ratio 0.55 and it is a shallow minimum. We may argue that the Ewald energy E'_{cc} plays a dominant role in determining the equilibrium axial ratio. The electronic contribution E_e serves as electronic screening and reduces the effect of the Ewald contribution. This is supported by the fact that the observed axial ratios are very close to the axial ratio of minimum Ewald energy.

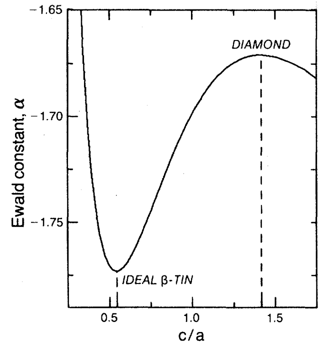

FIG. 13. Ewald constant of the β-tin phase as a function of axial ratio (c/a).

We note that the minima of E_{kin} and E'_H and the maxima of E'_{ec} and E_{xc} are also in the vicinity of axial ratio 0.55, which are related to the fact that the valence electrons are more uniformly distributed around that axial ratio.

In contrast, the Ewald contribution does not favor the diamond phase. Figure 13 plots the Ewald constant, which is proportional to the Ewald energy for a fixed volume, as a function of the axial ratio. While the observed β-tin phase is in the vicinity of a local minimum, the diamond phase corresponds to a local maximum.[50] This unfavorable Ewald contribution is more than compensated by the electronic contribution (E_e) for the diamond phase at Ω_{expt} as indicated in Fig. 14 in which we plot the differences between various contributions to the total energy of the diamond and the β-tin phase $(c/a=0.552)$ of Si as a function of atomic volume. Figure 14 also shows that E_{ec} and E_{xc} favor the diamond phase and E_{kin} and E'_H favor the β-tin phase. When the atomic volume decreases

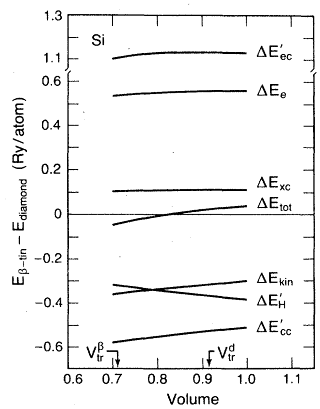

FIG. 14. Differences between various contributions to the total energy of the diamond phase and the β-tin phase $(c/a=0.552)$ of Si as a function of atomic volume (normalized to Ω_{expt}).

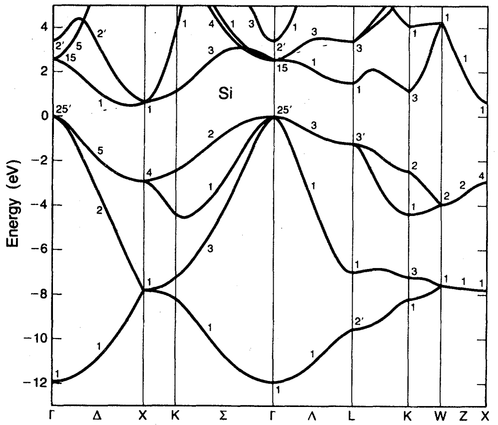

FIG. 15. Electronic structure of Si. Numbers refer to the conventional indices for symmetry group representations. Energies are measured from the valence-band maximum (Γ_{25}).

under pressure, the system becomes more metallic and the stabilizing effect of the electronic contribution (ΔE_e) for the diamond phase becomes weaker with respect to the opposing Ewald contribution ($\Delta E'_{cc}$). At the transition pressure, the gain in Ewald energy becomes so favorable relative to the β-tin phase that the phase transformation occurs, i.e., the Ewald contribution is the driving mechanism for this diamond$-\beta$-tin phase transformation.

D. Electronic structures

In this subsection, we present the results of electronic structure calculations for the diamond phase of Si and Ge at Ω_{expt}.[31] The electronic structures of Si and Ge shown in Figs. 15 and 16 are calculated using a plane-wave basis set with a kinetic-energy cutoff (E_{pw}) of 11.5 Ry at which point the overall convergent error of eigenvalues is about 0.05 eV. The s-like antibonding conduction state $\Gamma_{2'}$ has a large convergent error. It changes from 3.39 to 3.29 eV for Si and from 1.01 to 0.73 eV for Ge when E_{pw} is increased from 11.5 to 20 Ry. For $E_{\text{pw}}=20$ Ry, the overall convergent error of eigenvalues is 0.01 eV. (The Schrödinger equation is solved self-consistently for each E_{pw}.)

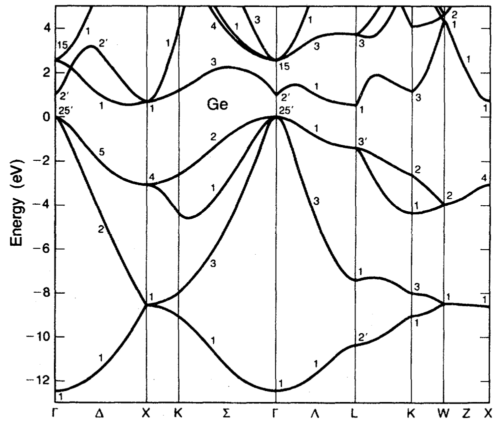

FIG. 16. Electronic structure of Ge (conventions of Fig. 15).

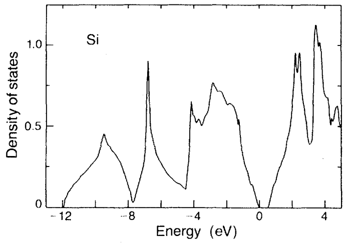

FIG. 17. Density of states of Si in units of state/eV atom. Energies are measured from the valence-band maximum.

In Table IX we listed the eigenvalues at Γ, X, and L of Si and Ge calculated using $E_{\text{pw}}=11.5$ and 20 Ry. These values agree quite well with other *ab initio* calculations.[34(c),45,51–53] In particular, the differences in eigenvalue between our results and the all-electron linearized augmented-plane-wave (LAPW) calculation[52] of Si are only about 0.1 eV.

Since the density-functional formalism was developed only for ground-state properties, the calculated eigenvalues do not correspond directly to elementary excitations. Nevertheless, a comparison of the calculated values with experimental excitation spectra may provide some clue to the construction of a fundamental theory for elementary excitations. The density of states for Si and Ge are displayed in Figs. 17 and 18. The peak positions agree quite well with the angle-integrated photoemission spectra.[54–56] In Table X, we compare our results with experiments at critical points. It seems that the calculated results can explain the peak posi-

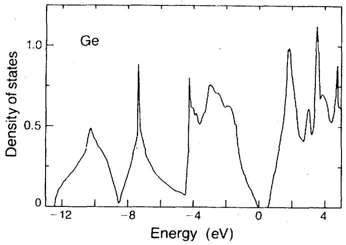

FIG. 18. Density of states of Ge (conventions of Fig. 17).

TABLE X. Comparison of the peak positions in the calculated valence-band density of states with those in angle-integrated photoemission spectra. Energies in eV are measured from the valence-band maximum.

	Si		Ge	
	Theory	Experiment	Theory	Experiment
Γ_1	-11.93	-12.4 ± 0.6^a -12.5 ± 0.6^b	-12.48	-12.6 ± 0.3^a -12.8 ± 0.4^b
$L_{2'}$	-9.52	-9.3 ± 0.4^b	-10.36	-10.6 ± 0.95^a -10.5 ± 0.4^b
L_1	-7.00	-6.4 ± 0.4^a -6.8 ± 0.2^b	-7.41	-7.7 ± 0.2^a -7.4 ± 0.2^b
Σ_1	-4.52	$-4.7\pm0.2^{a,b}$ -4.4^c	-4.51	$-4.5\pm0.2^{a,b}$
X_4	-2.88	-2.5 ± 0.3^b -2.9^c	-3.04	-3.2 ± 0.2^a
$L_{3'}$	-1.20	-1.2 ± 0.2^c	-1.39	-1.1 ± 0.2^a -1.4 ± 0.2^c

[a] Reference 55.
[b] Reference 54.
[c] Reference 56.

tions in the photoemission spectra rather well with an overall error of about 0.3 eV.

On the other hand, the comparison with the optical measurements shows large errors. The calculated indirect gaps are 0.48 eV from Γ to $0.85X$ for Si and 0.47 eV from Γ to L for Ge. The experimental values are 1.17 eV (Ref. 57) from Γ to $0.82X$ (Ref. 58) for Si, and 0.74 eV from Γ to L (Ref. 59) for Ge. While the calculated positions in the Brillouin zone for the valence-band maximum and the conduction-band minimum are in good agreement with experiment, the magnitudes of the energy gaps are underestimated. This seems to be a general phenomenon in the *ab initio* density-functional calculations. The calculated direct gaps are 2.54 eV ($\Gamma_{25'}\rightarrow\Gamma_{15}$) for Si and 0.73 eV ($\Gamma_{25'}\rightarrow\Gamma_{2'}$) for Ge. Again, these values are lower than the experimental values of 2.74 eV for Si (Ref. 60) and 0.89 eV for Ge,[61] but by a smaller amount (0.2 eV).

V. CONCLUSIONS

In summary we present an extensive microscopic study of the structural properties of two group-IV elemental crystals, Si and Ge, employing an *ab initio* pseudopotential method[18] within the local-density-functional formalism.[2] Using atomic numbers of the constituent elements and a subset of crystal structures (diamond, hexagonal diamond, β-tin, sc, bcc, hcp, and fcc) as the only input information, the calculated structural properties are in excellent agreement with experiment. They included (i) the static structural properties such as lattice constants, cohesive energies, and bulk moduli, (ii) the crystal stability such as the determination of the most stable phase, and (iii) properties of pressure-induced phase transformation.

In particular, our calculations show that the diamond phase of Si and Ge is the most stable phase among the seven phases under consideration and it will transform to the β-tin phase under hydrostatic pressure. The transition volumes and transition pressures, along with the axial ratio of the final β-tin phase in the pressure-induced phase transformation agree very well with experiment. We also show that the Ewald energy is the driving force for this pressure-induced diamond$-\beta$-tin phase transformation. The present results along with the results[1] of lattice-dynamical properties demonstrate that not only the static structural properties of crystals but also the other important structural properties of the crystal stability, phase transformation, and lattice dynamics can be accurately described from first principles within the local-density-functional formalism.

ACKNOWLEDGMENTS

This work was supported by the National Science Foundation under Grant No. DMR7822465 and by the Director, Office of Energy Research, Office of Basic Energy Sciences, Materials Sciences Division of the U. S. Department of Energy under Contract No. DE-AC03-76SF00098.

TABLE XI. Convergent test of the static properties of Si and Ge with respect to the kinetic-energy cutoff (E_{pw}) of the plane-wave basis set.

E_{pw} (Ry)	Lattice constant (Å)	Cohesive energy (eV/atom)	Bulk modulus (Mbar)
Si			
3.5	5.467	1.84	1.76
4.3	5.386	2.56	1.29
6.0	5.394	3.45	0.97
8.0	5.439	4.11	1.01
11.5	5.451	4.67	0.98
Expt.[a]	5.429	4.63	0.99
Ge			
6.0	5.551	2.41	0.89
8.0	5.599	3.24	0.79
11.5	5.655	4.02	0.73
Expt.[a]	5.652	3.85	0.77

[a] References 31, 32, and 33.

APPENDIX A

In this appendix, we give the results of the convergence test of the static properties with respect to the kinetic-energy cutoff (E_{pw}) for the plane-wave basis set (Table XI). The lattice constant converges quite fast, e.g., it has already converged to within 1% at $E_{\mathrm{pw}}=4.3$ Ry for Si. At $E_{\mathrm{pw}}=11.5$ Ry, the lattice constants converge to better than 1%, and the cohesive energies and the bulk moduli converge to about 5%.

APPENDIX B

In this appendix, we discuss the accuracy of the pseudopotential approximation in which an *ab initio* pseudopotential is used to simulate the interaction between the valence electrons and the atomic core. Shown in Fig. 19 is another *ab initio* pseudopotential of Si generated[22] using a reference configuration of $3s^2 3p^{0.5} 3d^{0.5}$, and r_c values (in a.u.) of 1.35, 1.56, and 1.56 for the s, p, and d components of the pseudopotential. While the pseudopotentials shown in Fig. 1(a) and Fig. 19 are quite different, the calculated equilibrium lattice constant, the cohesive energy, and the bulk modulus differ by only 0.5%, 1%, and 2% respectively. We have also tested other generation schemes[62] for *ab initio* pseudopotentials and obtained similar results. This demonstrates that the structural properties do not depend appreciably on the pseudopotential generating scheme and the parameters used in the scheme as long as the generated pseudopotential is capable of reproducing all-electron atomic results for a wide range of atomic configurations (see Sec. III).

We also note that the pseudopotential approximation works best for cases in which the valence wave functions do not overlap appreciably with the core wave functions as in the present case. When the overlaps are not negligible (e.g., in the case of Na), signficant error will result[63] from the fact that $V_{\mathrm{xc}}(\rho)$ [Eq. (10)] is a nonlinear function of the charge density. It has been shown[63] that such errors can be eliminated by including core-charge ef-

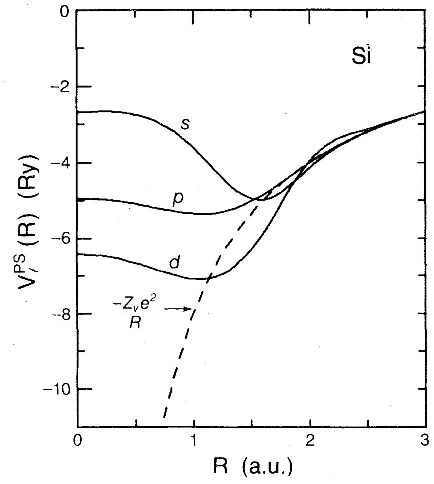

FIG. 19. *Ab initio* pseudopotential of Si generated using 1.35, 1.56, and 1.56 a.u. for r_c values of s, p, and d components.

fects in the treatment of the exchange-correlation potential and energy.

As for the core-core interaction energy, we consider it as purely electrostatic in our formalism. This approximation is quite accurate if the atomic cores do not overlap. Since 97% of the 2*s* (2*p*) core electrons of Si are within a sphere of radius 1.12 a.u. (1.15 a.u.), the value 1.2 a.u. is a good estimate of the core size of Si. Thus, the volume is to be compressed to $V_c/V_0=16\%$ of the free volume in the diamond phase and to even smaller volume in closely packed phases before the atomic cores overlap. Ge has relatively extended 3*d* core electrons and, hence, a larger core size. The value V_c/V_0 is about 30%. Therefore, the electrostatic approximation for the core-core interaction should be quite accurate for the volume compressions considered in the present study.

APPENDIX C

In this appendix, we examine the variation of the calculated structural properties with respect to the functional form of $E_{\text{xc}}[\rho]$. If the exchange-correlation form ($E_{\text{xc}}^{\text{HL}}$) proposed by Hedin and Lundqvist[64] (HL) is used in the calculation of the static properties of Si, the resulting lattice constant decreases by 1%, and the cohesive energy and the bulk modulus increase by 5% as compared to the corresponding results using the Wigner form E_{xc}^{W}.

The variations in the lattice constant and the cohesive energy can be qualitatively explained directly from the different functional forms of $E_{\text{xc}}[\rho]$. In the zeroth-order approximation, the exchange-correlation contribution to the total energy per atom is $Z_v\epsilon_{\text{xc}}(\bar{\rho})$ where Z_v is the number of valence electrons and $\bar{\rho}$ the average valence charge density. Compared with the Wigner form of ϵ_{xc}, the HL form decreases faster as $\bar{\rho}$ increases, viz., it favors a high charge density and small lattice constant. This also leads to a larger cohesive energy calculated using the HL form because the overall valence charge density of the crystal is larger than that of isolated atoms.

As for the study of crystal stability, $\Delta E_{\min}$ between the CD and the HD phases varies by less than 10^{-3} eV/atom when different E_{xc}'s are used. This is because both phases have almost the same equilibrium atomic volume and similar valence charge distributions. The difference $\Delta E_{\min}$ between the other five phases and the CD phase is lowered by about 0.02 eV/atom when $E_{\text{xc}}^{\text{HL}}$ is used instead of E_{xc}^{W}. This results from the fact that these five phases have smaller equilibrium atomic volume and that $E_{\text{xc}}^{\text{HL}}$ favors small atomic volumes. Such variations in $\Delta E_{\min}$ do not effect our conclusions about the crystal stability.

Since $E_{\text{xc}}^{\text{HL}}$ favors a small atomic volume, the calculated transition pressure for the diamond—β-tin phase transformation using $E_{\text{xc}}^{\text{HL}}$ is 10% smaller than that using E_{xc}^{W}. The transition volumes have only small variations, they decrease by 1% when $E_{\text{xc}}^{\text{HL}}$ is used instead of E_{xc}^{W}.

Other functional forms[30] of $E_{\text{xc}}[\rho]$ have also been examined, the results are similar to those discussed above. It should be noted that the expression of $E_{\text{xc}}[\rho]$ in Eq. (2) is itself an approximation (the local-density-functional approximation[2]).

---

[*] Present address: Bell Laboratories, Murray Hill, NJ 07974.

[1] (a) M. T. Yin and M. L. Cohen, Phys. Rev. Lett. 45, 1004 (1980); (b) M. T. Yin and M. L. Cohen, Solid State Commun. 38, 625 (1981).

[2] P. Hohenberg and W. Kohn, Phys. Rev. 136, B864 (1964); W. Kohn and L. J. Sham, *ibid.* 140, A1133 (1965).

[3] See, e.g., V. L. Moruzzi, J. F. Janak, and A. R. Williams, *Calculated Electronic Properties of Metals* (Pergamon, New York, 1978).

[4] S. Minomura and H. G. Drickamer, J. Phys. Chem. Solids 23, 451 (1962). The transition pressures reported are corrected by the revised calibration for high pressure [H. G. Drickamer, Rev. Sci. Instrum. 41, 1667 (1970)].

[5] J. C. Jamieson, Science 139, 762 (1963); 139, 845 (1963).

[6] See M. C. Gupta and A. L. Ruoff, J. Appl. Phys. 51, 1072 (1980) for a rather complete table of results of high-pressure studies on Si.

[7] G. J. Piermarini and S. Block, Rev. Sci. Instrum. 46, 973 (1975).

[8] B. A. Weinstein and G. J. Piermarini, Phys. Rev. B 12, 1172 (1975).

[9] K. Asaumi and S. Minomura, J. Phys. Soc. Jpn. 45, 1061 (1978).

[10] R. H. Wentorf and J. S. Kasper, Science 139, 338 (1962).

[11] C. H. Bates, F. Dachille, and R. Roy, Science 147, 860 (1965).

[12] F. P. Bundy and J. S. Kasper, Science 139, 340 (1963); J. S. Kasper and S. M. Richards, Acta Crystallogr. 17, 752 (1964).

[13] J. C. Phillips, Phys. Rev. Lett. 27, 1197 (1971); *Bonds*

and Bands in Semiconductors (Academic, New York, 1973).

[14] J. A. Van Vechten, Phys. Status Solidi B 47, 261 (1971); Phys. Rev. B 7, 1479 (1972).

[15] D. Penn, Phys. Rev. 128, 2093 (1962).

[16] A. Morita and T. Soma, Solid State Commun. 11, 927 (1972); T. Soma, J. Phys. C 11, 2681 (1978).

[17] W. Andreoni and K. Maschke, Phys. Rev. B 22, 4816 (1980).

[18] See, e.g., M. T. Yin and M. L. Cohen, Phys. Rev. B 25, 7403 (1982).

[19] A. K. McMahan, M. T. Yin, and M. L. Cohen, Phys. Rev. B 24, 7210 (1981).

[20] J. Ihm, A. Zunger, and M. L. Cohen, J. Phys. C 12, 4409 (1979); M. T. Yin and M. L. Cohen, Phys. Rev. B 26, 3259 (1982).

[21] See J. Ihm and M. L. Cohen, Phys. Rev. B 21, 3754 (1980), and references therein.

[22] D. R. Hamann, M. Schlüter, and C. Chiang, Phys. Rev. Lett. 43, 1494 (1979).

[23] E. Wigner, Phys. Rev. 46, 1002 (1934).

[24] M. Schlüter, J. R. Chelikowsky, S. G. Louie, and M. L. Cohen, Phys. Rev. B 12, 4200 (1975).

[25] D. J. Chadi and M. L. Cohen, Phys. Rev. B 8, 5747 (1973); H. J. Monkhorst and J. D. Pack, *ibid.* 13, 5189 (1976).

[26] O. Jepsen and O. K. Anderson, Solid State Commun. 9, 1763 (1971); G. Lehmann and M. Taut, Phys. Status Solidi B 54, 469 (1972).

[27] For the total-energy calculation of the bcc and fcc phases of Si reported in Ref. 1(a), the tetrahedron method was used. The convergent error was about 0.05 Ry/atom using 20 k points (for fcc) and 30 k points (for bcc) in the irreducible Brillouin zone. The present calculation for these two phases has a better convergency (0.001 Ry/atom).

[28] (a) F. D. Murnaghan, Proc. Nat. Acad. Sci. U.S.A. 30, 244 (1944); (b) O. L. Anderson, J. Phys. Chem. Solids 27, 547 (1966).

[29] We neglect the effect of lattice vibrations which is estimated to cause about 0.1% and 1% errors in the equilibrium lattice constant and the bulk modulus, respectively.

[30] U. von Barth and L. Hedin, J. Phys. C 5, 1629 (1972); O. Gunnarsson, B. I. Lundqvist, and J. W. Wilkins, Phys. Rev. B 10, 1319 (1974).

[31] The experimental zero-pressure lattice constants and atomic volumes (Ω_{expt}) at 0 K are obtained from J. Donohue, *The Structures of Elements* (Wiley, New York, 1974), corrected for thermal expansion and atmospheric-pressure compression.

[32] L. Brewer, Lawrence Berkeley Laboratory Report No. LBL-3720 (unpublished) (for the cohesive energy at 0 K); C. E. Moore, *Atomic Energy Levels* (National Bureau of Standards, Washington, D.C., 1949), Circular No. 467, Vol. I.

[33] H. J. McSkimin, J. Appl. Phys. 24, 988 (1953); H. J. McSkimin and P. Andreatch, Jr., *ibid.* 34, 651 (1963); 35, 2161 (1964). The elastic moduli were measured at 77 K.

[34] (a) J. A. Vergés and C. Tejedor, Phys. Rev. B 20, 4251 (1979); (b) A. Zunger, *ibid.* 21, 4785 (1980); (c) D. Glötzel, E. Segall, and O. K. Anderson, Solid State Commun. 36, 403 (1980).

[35] (a) A. Morita, T. Soma, and J. Takeda, J. Phys. Soc. Jpn. 32, 29 (1972); (b) H. Wendel and R. M. Martin, Phys. Rev. Lett. 40, 950 (1978); Phys. Rev. B 19, 5251 (1979); (c) J. Ihm and M. L. Cohen, Solid State Commun. 29, 711 (1979); Phys. Rev. B 21, 1527 (1980).

[36] J. F. Janak, V. L. Moruzzi, and A. R. Williams, Phys. Rev. B 12, 1257 (1975).

[37] G. Dolling, *Inelastic Scattering of the Neutrons in Solids and Liquids* (IAEA, Vienna, 1963), Vol. II, p. 37; G. Nilson and G. Nelin, Phys. Rev. B 3, 364 (1971).

[38] We have examined the convergency of the valence charge density with respect to E_{pw} (the kinetic-energy cutoff in the plane-wave expansion). The peak values (in units of electrons per atomic volume) changed from 11.7 to 11.5 for Si and from 11.35 to 11.3 for Ge when E_{pw} is increased from 11.5 to 20 Ry. The peak positions move away from the bond center in the bonding direction by about 4% of the bondlength for Si (5% for Ge). The changes in the valence contributions to the x-ray structural factors are about 0.01 e/cell.

[39] Y. W. Yang and P. Coppins, Solid State Commun. 15, 1555 (1974).

[40] P. J. E. Aldred and M. Hart, Proc. R. Soc. London Ser. A 332, 223 (1973).

[41] J. B. Roberto, B. W. Batterman, and D. T. Keating, Phys. Rev. B 15, 2590 (1974) [for the (222) reflection of Si].

[42] T. Matsushita and K. Kohra, Phys. Status Solidi A 24, 531 (1974).

[43] P. M. Raccah, R. N. Euwema, D. J. Stukel, and T. C. Collins, Phys. Rev. B 1, 765 (1970).

[44] R. Heaton and E. Lafon, J. Phys. C 14, 347 (1981).

[45] C. S. Wang and B. M. Klein, Phys. Rev. B 24, 3393 (1981).

[46] (a) L. Kaufman and H. Nesor, in *Titanium Science and Technology,* edited by R. I. Jaffe and H. Burte (Plenum, New York, 1973), Vol. 2, p. 773; (b) A. P. Miodownik, in *Metallurgical Chemistry, Proceedings of Metallurgical Chemistry Symposium, Brunel University and National Physical Laboratory, London,* edited by O. Kubaschewski (H.M.S.O., London, 1972). We thank Dr. D. G. Pettifor and Dr. L. Kaufman for bringing these empirical results to our attention.

[47] The pseudovalence charge density of the atom with configuration $3s^1 3p^3$ is used.

[48] See, e.g., T. L. Loucks, *Augmented Plane Wave Method* (Benjamin, New York, 1967).

[49] A. Jayaraman, W. Klement, Jr., and G. C. Kennedy, Phys. Rev. 130, 540 (1963); F. P. Bundy, J. Chem. Phys. 41, 3809 (1964).

[50] D. Weaire, Phys. Status Solidi 42, 767 (1970).

[51] D. J. Stukel and R. N. Euwema, Phys. Rev. B 1, 1635 (1970).

[52] D. R. Hamann, Phys. Rev. Lett. 42, 662 (1979).

[53] A. Zunger and M. L. Cohen, Phys. Rev. B 20, 4082 (1979).

[54] L. Ley, S. Kowalczyk, R. Pollak, and D. A. Shirley, Phys. Rev. Lett. 29, 1088 (1972). Their experimental values are quoted in J. R. Chelikowsky and M. L. Cohen, Phys. Rev. B 10, 5095 (1974).

[55] W. D. Grobman and D. E. Eastman, Phys. Rev. Lett. 29, 1508 (1972); W. D. Grobman, D. E. Eastman, and J. L. Freeouf, Phys. Rev. B 12, 405 (1975).

[56] W. E. Spicer and R. Eden, in *Proceedings of the Ninth International Conference of the Physics of Semiconductors, 1968* (Navka, Leningrad, 1968), Vol. 1, p. 61.

[57] K. L. Shalee and R. E. Nahony, Phys. Rev. Lett. 24, 942 (1970). The indirect band gap of Si was measured at 1.8 K.

[58] See W. P. Dunke, Phys. Rev. 118, 938 (1960), and references therein.

[59] C. Kittel, *Introduction to Solid State Physics*, 5th ed. (Wiley, New York, 1975), p. 210.

[60] G. K. M. Thutupalli and S. G. Tomlin, J. Phys. C 10, 467 (1977).

[61] H. Piller and V. A. Patton, Phys. Rev. 129, 1169 (1963).

[62] G. Kerker, J. Phys. C 13, L189 (1980).

[63] S. G. Louie, S. Froyen, and M. L. Cohen, Phys. Rev. B 26, 1738 (1982).

[64] L. Hedin and B. I. Lundqvist, J. Phys. C 4, 2064 (1971).